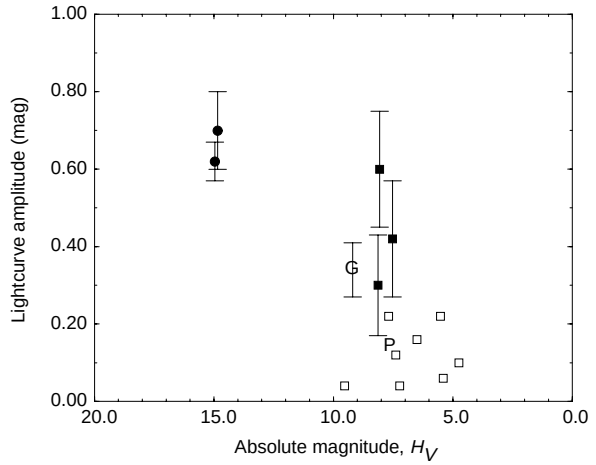

Figure 2 A plot of the light-curve amplitude versus the absolute magnitude for the 12 objects in our survey with good temporal coverage. The open squares and filled squares represent upper limits and Δm detections, respectively. The filled circles represent Δm detections for the bare nuclei of short-period comets[19,20]. The symbols P and G represent the Centaurs 5145 Pholus[10] and 1995 GO[3,11,21]. A pattern is clearly seen; intrinsically faint KBOs exhibit light curves.

around 250 km, assuming an albedo of 0.04. If we assume a density of 1 g cm^{-3}, we obtain a material strength of 8×10^6 dyn cm^{-2}, a value smaller than that of a bulk ice in a laboratory[14], 2×10^7 dyn cm^{-2}. Larger objects are known to be weaker than smaller objects of the same material. Models of size-dependent strength[15] imply that strength should scale as $R^{-3/(m+3)}$ where $m = 8.1$ for ice. Thus the models suggest that the strength of a KBO with $R = 100$ km should be $(10^7)^{-0.27} (= 0.01)$ times the laboratory strength of ice, that is, $\sim 2 \times 10^5$ dyn cm^{-2}.

The second possibility that can explain the trend in Fig. 2 is that the KBOs in our sample are all about the same size. The difference in intrinsic brightness would then be due to differences in albedo, the intrinsically faint objects being composed of a darker material than the brighter objects. If the dark material has a greater material strength than the lighter material, the dark objects could support more overlying material and hence retain their irregular shapes to greater diameters than could the light-coloured KBOs (E. Asphaug, personal communication).

What mechanism is responsible for the production of irregularly shaped objects? One possibility is that the objects in our survey retained their original shapes from the time they stopped growing. An alternative possibility is that the irregular shapes are shards from collisions. Calculations[16–18] have shown that objects with diameter >100 km cannot be shattered by collisions in the present-day Kuiper belt; this is because collisions between such large targets and impactors that are large enough to disrupt these targets are too infrequent. If the KBOs have albedos similar to those of short-period comets, then their irregular shapes are the result of primordial formation processes. □

Received 13 October 1998; accepted 4 January 1999.

1. Levison, H. F. & Weissman, P. R. in *The Encyclopedia of the Solar System* (eds Weisman, P. R., McFadden, L. A. & Johnson, T.) 557–582 (Academic, New York, 1999).
2. Bowell, E. B. *et al.* in *Asteroids II* (eds Binzel, R., Gehrels, T. & Matthews, M.) 524–556 (Univ. Arizona Press, Tucson, 1989).
3. Romanishin, W., Tegler, S. C., Levine, J. & Butler, N. BVR photometry of centaur objects 1995 GO, 1993 HA2, and 5145 Pholus. *Astron. J.* **113,** 1893–1898 (1997).
4. Tegler, S C. & Romanishin, W. Two distinct populations of Kuiper belt objects. *Nature* **392,** 49–51 (1998).
5. Tegler, S. C. & Romanishin, W. The extraordinary colors of 1994 TB and 1993 SC. *Icarus* **126,** 212–217 (1997).
6. Tegler, S. C. *et al.* Photometry of the trans-neptunian object 1993 SC. *Astron. J.* **114,** 1230–1233 (1997).
7. Hintzen, P., Romanishin, W. & Valdes, F. Galaxies clustering around QSOs with z = 0.9–1.5 and the origin of blue field galaxies. *Astrophys. J.* **366,** 7–15 (1991).
8. Trentham, N. The luminosity function of dwarf galaxies in four spiral-rich clusters. *Mon. Not. R. Astron. Soc.* **286,** 133–157 (1997).
9. Jewitt, D. & Luu, J. Optical-infrared spectral diversity in the Kuiper belt. *Astron. J.* **115,** 1667–1670 (1998).
10. Buie, M. W. & Bus, S. J. Physical observations of 5145 Pholus. *Icarus* **100,** 288–294 (1992).
11. Davies, J. K., McBride, N., Ellison, S. L., Green, S. F. & Ballantyne, D. R. Visible and infrared photometry of six centaurs. *Icarus* **134,** 213–227 (1998).
12. Schleicher, D. G. *et al.* Periodic variations in the activitiy of Comet P/Halley during the 1985/1986 apparition. *Astron. J.* **100,** 896–912 (1990).
13. Binzel, R., Farinella, P., Zappala, V. & Cellino, A. in *Asteroids II* (eds Binzel, R., Gehrels, T. & Matthews, M.) 416–441 (Univ. Arizona Press, Tucson, 1989).
14. Hobbs, P. V. *Ice Physics* (Clarendon, Oxford, 1974).
15. Asphaug, E. *et al.* Mechanical and geological effects of impact cratering on Ida. *Icarus* **120,** 158–184 (1996).
16. Stern, S. A. Collisional time scales in the Kuiper disk and their implications. *Astron. J.* **110,** 856–868 (1995).
17. Farinella, P. & Davis, D. R. Short-period comets: primordial bodies or collisional fragments? *Science* **273,** 938–941 (1996).
18. Stern, S. A. Signatures of collisions in the Kuiper disk. *Astron. Astrophys.* **310,** 999–1010 (1996).
19. Jewitt, D. C. & Luu, J. X. A CCD protrait of comet P/Tempel 2. *Astron. J.* **97,** 1766–1790 (1989).
20. Luu, J. X. & Jewitt, D. C. The nucleus of comet P/Encke. *Icarus* **86,** 69–81 (1990).
21. Brown, W. R. & Luu, J. X. CCD photometry of the Centaur 1995 GO. *Icarus* **126,** 218–224 (1997).

Acknowledgements. We thank D. Schleicher for application of his phase dispersion minimization and phasing software to the KBO lightcurves, and E. Asphaug and J. Davies for comments on the manuscript. We also thank the Steward Observatory Telescope Allocation Committee for telescope time. This work was supported by the NASA Origins of Solar Systems and Planetary Astronomy programs.

Correspondence and requests for materials should be addressed to W.R. (e-mail: wjr@mail.nhn.ou.edu).

Quantum-well states in copper thin films

R. K. Kawakami*, E. Rotenberg†, Hyuk J. Choi*, Ernesto J. Escorcia-Aparicio*, M. O. Bowen*, J. H. Wolfe*, E. Arenholz*, Z. D. Zhang*‡, N. V. Smith† & Z. Q. Qiu*

* *Department of Physics, University of California at Berkeley, Berkeley, California 94720, USA*

† *Advanced Light Source, Lawrence Berkeley National Laboratory, Berkeley, California 94720, USA*

A standard exercise in elementary quantum mechanics is to describe the properties of an electron confined in a potential well. The solutions of Schrödinger's equation are electron standing waves—or 'quantum-well' states—characterized by the quantum number *n*, the number of half-wavelengths that span the well. Quantum-well states can be experimentally realized in a thin film, which confines the motion of the electrons in the direction normal to the film: for layered semiconductor quantum wells, the aforementioned quantization condition provides (with the inclusion of boundary phases) a good description of the quantum-well states. The presence of such states in layered metallic nanostructures is believed to underlie many intriguing phenomena, such as the oscillatory magnetic coupling of two ferromagnetic layers across a non-magnetic layer[1,2] and giant magnetoresistance[3]. But our understanding of the properties of the quantum-well states in metallic structures is still limited. Here we report photoemission experiments that reveal the spatial variation of the quantum-well wavefunction within a thin copper film. Our results confirm an earlier proposal[4] that the amplitude of electron waves confined in a metallic thin film is modulated by an envelope function (of longer wavelength), which plays a key role in determining the energetics of the quantum-well states.

The standard quantization condition on an electron of wavevector k within a potential well of width d is:

$$2kd + \phi = 2\pi n \qquad (1)$$

This equation expresses the requirement that, as the electron 'bounces' back and forth within the well, the length of a round trip must (apart from end corrections embodied in the phase ϕ) equal an integral number of wavelengths. For fixed n, an increase of d results in a decrease of k. Because the conduction electron's

‡ Permanent address: International Center for Materials Physics, Institute of Metal Research, Academia Sinica, Shenyang 110015, People's Republic of China.

energy usually increases with increasing k in noble metals (for example, in Cu, Ag and Au), equation (1) implies a decrease of the quantum-well (QW) energy with increasing d. However, previous photoemission experiments on metallic QW states show that the QW energies in fact increase with increasing film thickness[4–6]. This apparent contradiction can be circumvented[5] by rewriting equation (1) in terms of a new quantum number ν:

$$2(k_{BZ} - k)d - \phi = 2\pi\nu \qquad (2)$$

where $k_{BZ} = \pi/a$ is the Brillouin-zone vector, a is the atomic spacing, $\nu = m - n$, and m is the number of atomic layers within the well. Equation (2) now gives an *increase* of the QW energy with increasing d, as observed experimentally. Is this merely a book-keeping trick, or is there some underlying physical significance? Noting that the electron wavevectors near the Fermi level in metals are close to the Brillouin-zone boundary ($k \approx k_{BZ}$), it has been proposed[4] that electron waves under this situation should carry an envelope function with wavevector ($k_{BZ} - k$) that modulates the amplitude of the fast oscillating electron wave, as illustrated schematically in Fig. 1. Thus, equation (2) represents the quantization condition of the envelope function, with the quantum number ν simply being the number of nodes of the envelope function.

To investigate this idea experimentally, we developed a technique for mapping the spatial variation of the wavefunction in a QW. The method is analogous to sensing the standing-wave nodal structure of a vibrating string by lightly touching the string at different positions: touching the string at an antinode causes considerable damping of the vibration, but touching the string at a node has little effect. Thus by systematically changing the contact position along the string, it is possible to map out the spatial variation of the vibration amplitude for a given vibrational mode. For the case of the Cu QW state, the analogue of the 'touch' is provided by a thin Ni film (~1 monolayer, ML) inserted into the Cu QW. We chose Ni as the 'touch' layer for both structural and electronic reasons. Structurally, Ni shows pseudomorphic growth on Cu(100) so that it should not significantly affect the epitaxial growth of the Cu layer. Electronically, the band structure of Ni is sufficiently different from that of Cu that it offers an effective barrier to the free propagation of electrons between the Cu layers. By inserting the Ni layer into different positions of the Cu QW, it should therefore be possible to map out the spatial variation of the envelope function for a given QW state. Experimentally, the samples were prepared in ultrahigh vacuum (~10^{-10} torr). A 15 ML Co layer was first grown onto a Cu(100) single crystal to serve as the Co substrate. The Cu QW was then built by epitaxially growing the Cu film onto the Co substrate[6]. To vary systematically the Ni position within the Cu QW, we fabricated a double-wedge sample as illustrated in Fig. 2a: two identical Cu wedges were tapered in directions at right angles, with 1 ML Ni grown in between. Moving along the diagonal direction BD, the total Cu thickness is constant, but the Ni layer is swept continuously from one side of the Cu QW to the other to sense the expected envelope function. Moving along the other diagonal, AC, has the effect of varying the total Cu thickness while keeping the Ni barrier in the centre. We shall consider both BD and AC variations.

Photoemission spectroscopy is an ideal tool for the QW study because the photoemission intensity is proportional to the number of electrons at the given energy (the density of states). Thus, the QW states (which exist only at certain discrete energy levels) will manifest themselves as peaks in the photoelectron energy spectrum. Our photoemission experiments were performed at the Advanced Light Source, and take advantage of the high brightness of this third-generation synchrotron radiation facility. A high photon flux (> 10^{12} photons s^{-1}) can be delivered into a small spot size (50–100 μm) on the sample. Combining this with the use of wedge-shaped samples (Fig. 2a), it is possible to investigate a range of layer thicknesses by moving the wedge sample laterally through the illuminated spot. Figure 2b shows the photoemission intensity at the Fermi level across the sample. Two types of oscillations are visible. Scanning vertically (that is, parallel to AC), we see oscillations having a period of 5.6 ML. This oscillation has been seen before[4,6], and the intensity peaks correspond to the QW states with different index ν at the Fermi level within the Cu film. Scanning horizontally (that is, parallel to BD), we see oscillations that have not been seen before: each QW state labelled by index ν now oscillates as the Ni layer is swept through the Cu film. Qualitatively, these oscillations reflect the spatial variation of the envelope function of the Cu QW states as sensed by the Ni layer. For further understanding it is necessary to consider the wavefunction matching conditions at the boundaries embodied in the phase ϕ. It turns out in our case that ϕ is small, which means that the envelope function is 'trying' to place its antinodes at the boundaries[4]. In the

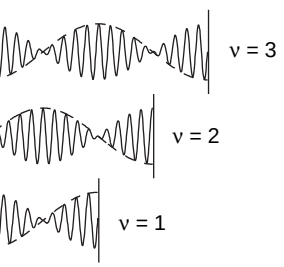

Figure 1 Schematic drawing of the QW wavefunctions at a given energy for $\nu = 1$, 2 and 3. The amplitude of the fast-oscillating electron wave is modulated by the envelope function (dashed line).

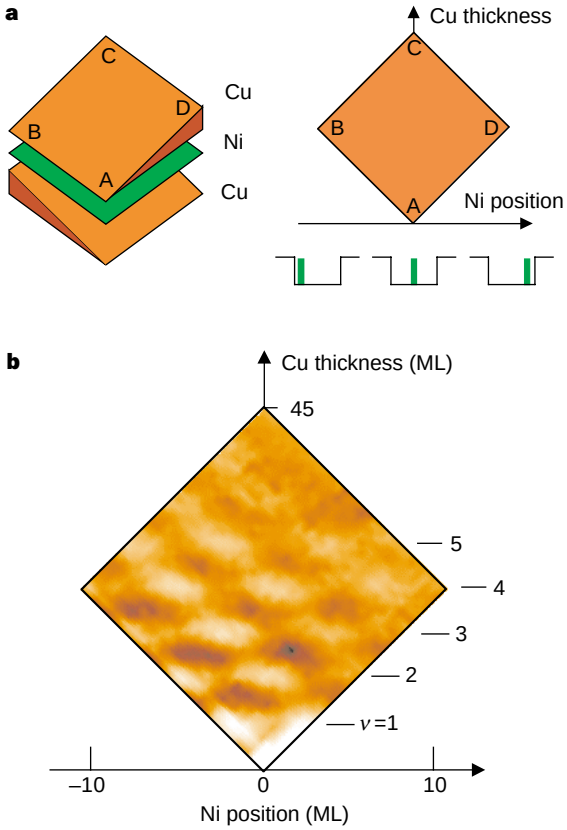

Figure 2 Spatial variation of the QW wavefunctions mapped by photoemission. **a**, Schematic drawing of the double-wedge sample that allows independent variation of the Ni layer position and the total Cu thickness. **b**, The two-dimensional image of the normal-emission photoemission intensity at the Fermi level taken over the double-wedge. The intensity variation with the Ni position reflects the QW envelope function as shown in Fig. 1.

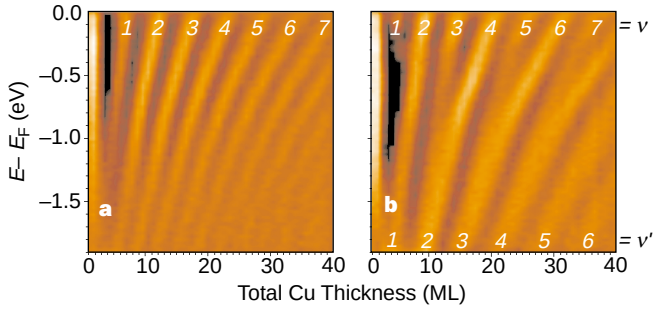

Figure 3 Images of the photoemission energy spectra versus the total Cu thickness for the symmetrical double QW Cu/Ni/Cu. **a**, 0 ML Ni; **b**, 1 ML Ni. With the presence of the Ni, each degenerate QW state at low energy splits into two states at high energy with even and odd parities.

presence of the Ni barrier, the QW states will be least perturbed when the barrier is itself near an antinode of the envelope function. When the barrier is close to a node of the envelope function, there will be difficulty in satisfying the wavefunction matching condition, leading to a damped or suppressed QW state. Thus the maximum and minimum intensities in the scans parallel to BD correspond respectively to the antinodes and nodes of the envelope function, and we associate the $\nu = 1, 2, 3$ states in Fig. 2b with the schematic wavefunctions of Fig. 1.

When the Ni barrier is at the centre of the Cu (along line AC in Fig. 2a), it separates the Cu layer into a symmetric double QW system. This spatial symmetry requires that the envelope function is either symmetric (even parity with an antinode at the centre) or antisymmetric (odd parity with a node at the centre) relative to the centre of the well. The parity of the envelope function has the observable consequence, as can be seen along the AC line in Fig. 2b, that QW states of even ν are more intense than those of odd ν. We now examine this in more detail at different electron energies. Noting that the Ni serves as a potential energy barrier, the propagation of the Cu electron wave across the Ni layer should become more difficult at lower energies. This is associated with a bandgap of bulk Ni (at ~1 eV below the Fermi level) within which free propagation of electrons is prohibited[7]. Thus, we expect the following two limiting cases based on elementary quantum mechanics. At low energies, the Ni barrier will completely decouple the two Cu QWs to result in degenerate QW states in the two Cu wells. At high energies, the degeneracy of the QW states in the two Cu wells will be lifted by the propagation of the Cu electrons across the Ni barrier, resulting in two non-degenerate QW states with odd and even parities. Figure 3b shows the evolution of the QW states at different energies with 1 ML Ni at the centre of the Cu well (Fig. 3a shows the case without the Ni barrier for comparison). At low energies ($E - E_F < -1$ eV, where E_F is the Fermi energy), we see the degenerate QW states of the separated Cu wells labelled by the quantum number ν'. As the energy increases, we see these states split into pairs. As compared with Fig. 3a, which corresponds to the case with no Ni barrier, the degenerate states labelled by ν' evolve into the $\nu = 2\nu' - 1$ and $\nu = 2\nu'$ states of the Cu well of twice the thickness. Figure 3b therefore demonstrates that the coupling of the two Cu QWs results in pairs of QW states with odd and even parities.

The qualitative analysis presented here needs to be tested with quantitative theoretical calculation. For example, tight-binding modelling[5] might provide useful insight into the orbital character of the QW wavefunctions. The aim is to reach a level of theoretical understanding and experimental control that will enable us to consider 'wavefunction engineering' of metallic layered systems, comparable to the 'bandgap engineering' that is now well established in semiconductor layered structures. □

Received 24 September 1998; accepted 5 January 1999.

1. Grünberg, P., Schreiber, R., Pang, Y., Brodsky, M. B. & Sowers, H. Layered magnetic structures: evidence for antiferromagnetic coupling of Fe layers across Cr interlayers. *Phys. Rev. Lett.* **57,** 2442–2445 (1986).
2. Parkin, S. S. P., More, N. & Roche, K. P. Oscillations in exchange coupling and magnetoresistance in metallic superlattice structures: Co/Ru, Co/Cr, and Fe/Cr. *Phys. Rev. Lett.* **64,** 2304–2307 (1990).
3. Baibich, M. N. *et al.* Giant magnetoresistance of (001)Fe/(001)Cr magnetic superlattices. *Phys. Rev. Lett.* **61,** 2472–2475 (1988).
4. Ortega, J. E. & Himpsel, F. J. Quantum well states as mediators of magnetic coupling in superlattices. *Phys. Rev. Lett.* **69,** 844–847 (1992).
5. Smith, N. V., Brookes, N. B., Chang, Y. & Johnson, P. D. Quantum-well and tight-binding analyses of spin-polarized photoemission from Ag/Fe(001) overlayers. *Phys. Rev. B* **49,** 332–338 (1994).
6. Kawakami, R. K. *et al.* Observation of the quantum well interference in magnetic nanostructures by photoemission. *Phys. Rev. Lett.* **80,** 1754–1757 (1998).
7. Mankey, G. J., Willis, R. F. & Himpsel, F. J., Band structure of the magnetic fcc pseudomorphs: Ni(100), Co(100), and Fe(100). *Phys. Rev. B* **48,** 10284–10291 (1993).

Acknowledgements. This work was supported by the US DOE, the US National Science Foundation, and the University of California for the conduct of discretionary research by Los Alamos National Laboratory. Z.D.Z. acknowledges the support of the National Science Foundation of China. E.A. acknowledges the support of the Miller Institute at the University of California, Berkeley.

Correspondence and requests for materials should be addressed to Z.Q.Q. (e-mail: qiu@socrates.berkeley.edu).

Enhancement of surface self-diffusion of platinum atoms by adsorbed hydrogen

S. Horch*, H. T. Lorensen†, S. Helveg*, E. Lægsgaard*, I. Stensgaard*, K. W. Jacobsen†, J. K. Nørskov† & F. Besenbacher*

** Center for Atomic-scale Materials Physics (CAMP), and Institute of Physics and Astronomy, University of Aarhus, DK 8000 Aarhus C, Denmark*
† CAMP and Physics Department, Technical University of Denmark, DK 2800 Lyngby, Denmark

Surface diffusion of atoms is an important phenomenon in areas of materials processing such as thin-film growth and sintering. Self-diffusion (that is, diffusion of the atoms of which the surface is comprised) has been much studied on clean metal and semiconductor surfaces[1,2]. But in most cases of practical interest the diffusion happens on surfaces partly covered by atoms and molecules adsorbed from the gas phase. Adsorbed hydrogen atoms are known to be capable of both promoting and inhibiting self-diffusion[3–7], offering the prospect of using adsorbed gases to control growth or sintering processes[8–11]. Here we derive mechanistic insights into this effect from observations, using the scanning tunnelling microscope, of hydrogen-promoted self-diffusion of platinum on the Pt(110) surface. We see an activated Pt–H complex which has a diffusivity enhanced by a factor of 500 at room temperature, relative to the other Pt adatoms. Our density-functional calculations indicate that the Pt–H complex consists of a hydrogen atom trapped on top of a platinum atom, and that the bound hydrogen atom decreases the diffusion barrier.

We have studied the influence of gas adsorbates on the diffusion of metal adatoms on the reconstructed Pt(110)-(1 × 2) surface, for which every second close-packed Pt row is missing (Fig. 1). This is an ideal model system because the motion of Pt adatoms is one-dimensional and is restricted to the troughs between close-packed rows of Pt atoms.

The experiments were performed in a standard ultrahigh vacuum system equipped with a fast-scanning, variable-temperature scanning tunnelling microscope (STM) that was built in our laboratory at the University of Aarhus. Platinum adatoms were deposited onto the clean (1 × 2) reconstructed surface by heating a 99.995% pure Pt wire. Hydrogen was coadsorbed from a constant background pressure.

To gain detailed insight into the migration of the Pt adatoms, we have acquired a large number of consecutive STM images